Received: 30 January 2018 | Accepted: 12 June 2018

DOI: 10.1002/mds3.10003

ORIGINAL ARTICLE

WILEY

SERS sensing of perampanel with nanostructured arrays of gold particles produced by pulsed laser ablation in water

Marco Santoro[1] | Enza Fazio[1] | Sebastiano Trusso[2] | Matteo Tommasini[3] | Andrea Lucotti[3] | Rosalba Saija[1] | Marina Casazza[4] | Fortunato Neri[1] | Paolo Maria Ossi[5]

[1]Dipartimento di Scienze Matematiche e Informatiche, Scienze Fisiche e Scienze della Terra, Università di Messina, Messina, Italy

[2]CNR-IPCF Istituto per i Processi Chimico-Fisici, Messina, Italy

[3]Dipartimento di Chimica, Materiali, Ingegneria Chimica, Politecnico di Milano, Milano, Italy

[4]Fondazione IRCCS istituto Neurologico "C.Besta", Milano, Italy

[5]Dipartimento di Energia & Center for NanoEngineered Materials and Surfaces-NEMAS, Politecnico di Milano, Milano, Italy

Correspondence
Enza Fazio, Dipartimento di Scienze Matematiche e Informatiche, Scienze Fisiche e Scienze della Terra, Università di Messina, Viale Ferdinando Stagno d'Alcontres 31, 98166 Messina, Italy.
Email: enfazio@unime.it
and
Paolo Maria Ossi, Dipartimento di Energia & Center for NanoEngineered Materials and Surfaces-NEMAS, Politecnico di Milano, Via Ponzio 34-3, 20133 Milano, Italy.
Email: paolo.ossi@polimi.it

Funding information
Polisocial Award 2013–2014

Abstract

Noble metal nanoparticles (NPs) are among the most extensively studied colloidal systems, due to their surface plasmon resonances (SPR) of interest for biological sensing. We report here the synthesis of Au nanoparticles as water-based colloids by nanosecond (τ = 5 ns) and picosecond (τ = 6 ps) pulsed laser ablation at the fixed fluence of 1.5 J/cm^2 (λ = 532 nm) and different irradiation times (20 minutes, ns irradiations; 5 minutes, ps irradiations). Both ns and ps ablation lead to the synthesis of highly stable and chemically pure NPs. ps pulses allow synthesizing in remarkably short times (few minutes) smaller NPs with a narrower size distribution than using ns pulses. The surface-enhanced Raman scattering (SERS) activity of Au NPs produced by ps ablation was tested, obtaining the first SERS spectrum of the new generation antiepileptic drug perampanel, whose clinical interest is relevant.

KEYWORDS
antiepileptic drug, perampanel, plasmonic nanoparticle, pulsed laser ablation, surface-enhanced Raman spectroscopy

1 | INTRODUCTION

Nanometre-sized gold (Au) structures find widespread use for application in optics in the visible range thanks to their remarkable ability to enhance local electromagnetic fields through plasmon resonance effects (Fazio, Trusso, & Ponterio, 2013; Indrasekara et al., 2013; Tian et al., 2015). Conventional fabrication of gold colloids is often accomplished by multistep chemical synthesis that results in rather long production times (hours to days) and requires multiple purification steps. Although 5–100 nm NPs are produced by a fairly direct chemical reduction method, their surface is likely to be covered by reaction by-products such as anions and reducing agents that can affect the subsequent stabilization and functionalization steps (Zeng et al., 2011).

By photo-assisted synthesis methods, a comparatively fast production of metal NPs is possible. The methods can be split into photophysical and photochemical. In photochemical methods (Sakamoto, Fujistuka, & Majiam, 2009), light, usually in the UV region, induces photoreduction of a metal salt. Gold and silver NPs are generated by photoreduction of $AuCl^{4-}$ and $AgClO_4$, respectively (Hada, Yonezawa, Yoshida, & Kurakake, 1976; Kurihara, Kizling, Stenius, & Fendler, 1983). For both metals, NPs are generated in a medium containing chemical residues of the reduction reaction.

Photophysical methods are based on the vaporization of a solid target by high-energy laser pulses. The process is performed in an ambient fluid, either gas or liquid, whose role is to confine the vaporized species and to induce their aggregation in clusters and NPs.

The method has the advantage to produce NPs free from any chemical precursor. When the process is performed in an ambient gas at high pressure (Fazio, Neri, Ossi, Santo, & Trusso, 2009), NPs possibly coalesced are grown as arrays onto appropriate rigid flat supports; when liquids are used as the confining medium, a colloidal solution is obtained. The conceptually simple pulsed laser ablation in liquid (PLAL) technique, using nano/picosecond laser pulses, allows to produce surfactant-free NPs in a single step within a time scale of a few minutes (Acacia et al., 2010; Mafunè, Kohno, Takeda, & Kondow, 2000). The laser pulse deposits a large energy density at a focused spot on the target surface leading to ablation from the target of matter that immediately converts to a plasma that consists of both ablated species and a small amount of water molecules. Such a plasma plume expands through the liquid that spatially confines it. The high temperatures (of the order of thousands of Kelvin) and pressures (in the range of GPa) attained inside the plume during the regime of collisional expansion allow for NP formation. The low production yield of NPs, the purity and redispersibility from agglomerates is present limitations of PLAL (Barcikowski, Hahn, Kabashin, & Chichkov, 2007). Over the last decade, major efforts were directed to produce stable solutions of small NPs with narrow size distributions and controlled surface chemistry for biomedical applications (Dreaden, Alkilany, Huang, Murphy, & El-Sayed, 2012). Pulsed laser ablation in liquid appears among the most flexible and promising methods of NP synthesis because of the independent control of relevant process parameters such as irradiation time, energy density, laser wavelength, and because the ultra-high deposited energy density permits to ablate almost all kinds of materials. For ns-PLAL, we analysed the irradiation geometry, finding optimal focusing conditions to maximize the ablation rate (Fazio & Neri, 2013). For noble metals and ceramics, more recent systematic investigations compared the morphology, size, size distribution, production yield, absorption spectra of NPs produced by ns-, ps- and fs-PLAL at different laser wavelengths (Hamad, Li, & Liu, 2015). Compared to ns lasers, high repetition rate ps lasers are advantageous whenever the total thermal load produced by laser irradiation can be redistributed over a larger area (Ostendorf, Kamlage, Klug, Korte, & Chichkov, 2005). When laser ablation is carried out in a polar liquid (typically, water), surface-charged NPs are produced. These are solvated by a shell of dipolar molecules (e.g., water) and do not agglomerate because of the Coulomb repulsion generated by their surface charge (Fazio et al., 2016).

The SPR depends on the structural and morphological properties of the noble metal NPs, thus it is necessary to determine the appropriate ablation parameters to obtain NPs with tailored size distributions and concentration (Fazio et al., 2009; Ossi & Bailini, 2008). In this work, moving from our previous results (Fazio & Neri, 2013), we report on the use of ns (λ = 532 nm; τ = 5 ns) and ps (λ = 532 nm; τ = 6 ps) PLAL at optimized fluence and irradiation times to synthesize Au NPs in water. By ns- and ps-PLAL, we obtained stable and pure NPs in colloidal state, with variable size and optical properties. After ultrasonically spraying a fraction of such Au colloids on inert glass or (100) Si supports, we obtained Au NP arrays with specific surface nanostructure. Such films were tested as SERS substrates against the antiepileptic drug perampanel which is the active pharmaceutical ingredient (API) of Fycompa® (Patsalos, 2015). Fycompa is indicated for the adjunctive treatment both of partial-onset seizures with or without secondarily generalized seizures and of primary generalized tonic–clonic seizures in adult and young patients from 12 years of age. The European Commission authorized Fycompa commercialization throughout EU Countries on 2 July 2015. Perampanel, being the progenitor of a new class of antiepileptic drugs, offers to epileptologists new therapeutic opportunities in the treatment of farmaco-resistant epilepsy (Krauss et al., 2013). As an example, 90 adult patients are presently treated with Fycompa at I.R.C.C.S. Fondazione Istituto Neurologico "C. Besta," Milano, Italy (data provided by UO Neurofisiopatologia, I.R.C.C.S. Fondazione Istituto Neurologico "C.Besta," Milano, Italy). Perampanel is a first-in-class selective, non-competitive antagonist of the ionotropic α-amino-3-hydroxy-5-methyl-4-isoxazolepropionic acid (AMPA) glutamate receptor on post-synaptic neurons (Rogawski, 2011). Glutamate is the primary excitatory neurotransmitter in the central nervous system and is implicated in a number of neurological disorders caused by neuronal over-excitation (Rogawski & Hanada, 2013). Activation of AMPA receptors by glutamate is thought to be responsible for most fast-excitatory synaptic transmission in the brain (Patsalos, 2015). In vivo, perampanel significantly prolonges seizure latency in an AMPA-induced seizure model. Presently, the detailed mechanism by which perampanel exerts its antiepileptic effects in humans is still to be fully elucidated (Patsalos, 2015).

2 | METHODS

Au colloids were prepared by pulsed laser ablation using 532 nm radiation provided by the second harmonic of a Nd:YAG source with a repetition rate of 10 Hz and pulse width of 5 ns as well as by an ultra-fast Nd:YVO_4 source with repetition rate of 10^2 kHz and pulse duration of 6 ps. The pulsed, high-power laser beam impacts onto a rod-shaped Au target (99.99% purity) immersed in demineralized water (see Figure 1). The optimized ablation times ensuring high NP productivity were 20 min (ns-PLAL) and 5 min (ps-PLAL); for both conditions, the laser fluence was F = 1.5 J/cm^2 (Fazio & Neri, 2013).

The Au content in colloids was determined by graphite furnace atomic absorption spectroscopy (GF-AAS) using a Varian 220/Zeeman atomic absorption spectrometer, equipped with a single-element hollow cathode lamp and a Varian PSD autosampler. The quantification of Au was carried out using the external standard method. The analytical method was validated according to the ICH guidelines (ICH Harmonised Tripartite Guideline Validation of Analytical Procedures: Text and Methodology Q2(R1), 2005). The linearity was >0.999, the precision (expressed as relative standard deviation) 0.560, and the detection limit 8.0 ng/ml. The reported data are the average out of three determinations.

We recorded UV–Vis spectra of the colloids using quartz cells and a Perkin Elmer Lambda 750 UV–Vis spectrometer working in

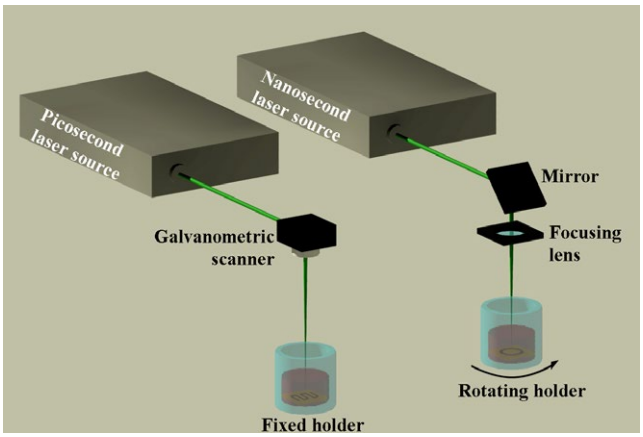

FIGURE 1 Scheme of laser ablation set-up using a ps and a ns laser source. In the latter set-up, the rotating holder helps minimizing cratering of the target

the 300–900 nm range. Colloids were deposited on a nickel grid to carry out scanning transmission electron microscopy (STEM) using a Merlin model ZEISS-Gemini 2 instrument operating at primary voltage of 30 kV at the working distance of 4 mm.

FT-Raman measurements were carried out with a Nicolet NXR9650 instrument equipped with a solid-state Nd-YVO_4 laser providing the excitation wavelength of 1064 nm with the laser power at the sample of about 1.4 W, on a spot of 50 μm diameter. To test the SERS activity of Au NPs produced by ps-PLAL, a fraction of the colloids was ultrasonically sprayed on (100) Si supports. On the resulting films, we carried out SERS measurements of the antiepileptic drug perampanel extracted from a Fycompa tablet. SERS measurements were carried out with a micro-Raman Labram HR800 instrument (Horiba-Jobin Yvon) equipped with a 785 nm solid-state laser XTRA Toptica Photonics with the laser power at the sample of about 5 mW. The beam was focused by a 50× objective of an Olympus BX41 microscope in a spot of about 1 μm diameter. For SERS measurements, the core of a 6 mg Fycompa tablet was grinded to obtain about 5 mg of API (perampanel) mixed together with slightly less than 200 mg of excipients (predominant excipient, lactose monohydrate (http://www.ema.europa.eu/docs/it_IT/document_library/EPAR_Product_Information/human/002434/WC500130815.pdf); see Figure 6 for details on the other excipients). The obtained powder was cast in 10 ml of methanol, to which 0.2 ml of HCl 37% was added to foster protonation of perampanel and help solubilizing it. The insoluble solid deposit was removed from the suspension by centrifugation. Based on the adopted solvent volumes, and supposing that the whole 5 mg of perampanel was dissolved, we estimate a (maximum) final 1.4×10^{-3} M concentration of perampanel in methanol. The Au SERS sensor supported on Si (see spraying procedure) was fully dip into a few ml of the 1.4×10^{-3} M perampanel solution for 1 minute. Then, the sensor was extracted from the solution and let dry in ambient air for 10 minutes before carrying out micro-Raman measurements.

X-ray diffraction (XRD) was performed by a Bruker instrument using Cu K_α radiation (0.15406 nm).

3 | RESULTS AND DISCUSSION

3.1 | Au nanoparticle synthesis and characterization

We obtained Au NPs with narrow size distribution using both ns and ps laser pulses. The latter allow for a higher NP productivity, as indicated by the SPR profile (Figure 2e, red line) which is more intense and slightly narrower than that collected from NPs produced by ns pulses.

Compared with ns-NPs, a narrowing of the SPR peak for the ps-NPs as well as an increase in the background is observed, while the SPR position is practically unaffected (Figure 2e). The narrowing depends on the presence of small, isolated NPs, while the background increase is due to a larger NP yield. Both features agree with STEM images (Figure 2a,b) and the size histograms in Figure 2c,d (see Table 1 for details on the fitting procedure of the size distribution).

We remark that we kept fixed the laser fluence and wavelength so that we could better compare NP sizes and production yields between ns and ps synthesis conditions with respect to previous studies (Hamad et al., 2015), assuming that NP size is mostly affected by the laser wavelength, whereas production yield is mostly affected by the laser fluence (Hamad et al., 2015).

Our results can be interpreted by considering that laser ablation in a stationary liquid involves the simultaneous production of NPs by ablation of the target material and the fragmentation/assembling of dispersed NPs by continuous irradiation of the already synthesized particles. In this respect, pulse duration is a relevant parameter for NP generation (Schwenke, Wagener, Nolte, & Barcikowski, 2011). By changing the pulse duration from ns to ps, the relevance of melting and thermal evaporation among ablation mechanisms significantly decreases. The shorter the pulse duration, the more efficient the ablation process that involves a nearly instantaneous evaporation with a minimized heat affected zone (Kelly & Miotello, 1996; Momma et al., 1996), thus resulting in a shorter time to produce the colloids. Furthermore, primary plasma shielding that is detrimental to ablation efficiency is much reduced with ps laser pulses, as compared to ns pulses (Pathak & Povitisky, 2008).

X-ray diffraction data in Figure 3 show that the NPs prepared by ps-PLAL are crystalline, as confirmed by the (111), (200), (220) and (311) Bragg reflections of fcc Au (see card JCPDS 04-0784). (111) texture is present. The XRD features are broader than those in Au nanocrystals (Sneha, Sathishkumar, Kim, & Yun, 2010). Most likely, this is due to a combination of the small size of such particles (see Figure 2d) with the associated residual stresses.

3.2 | Time evolution of colloids

Dynamic light scattering (DLS) allows to estimate the changes in size and size distribution of the particles. DLS data systematically correlate with the changes in the SPR lineshapes observed by UV–Vis spectroscopy. Au colloids produced by both ns- and ps-PLAL were stored for 3 months at atmospheric conditions; thereafter,

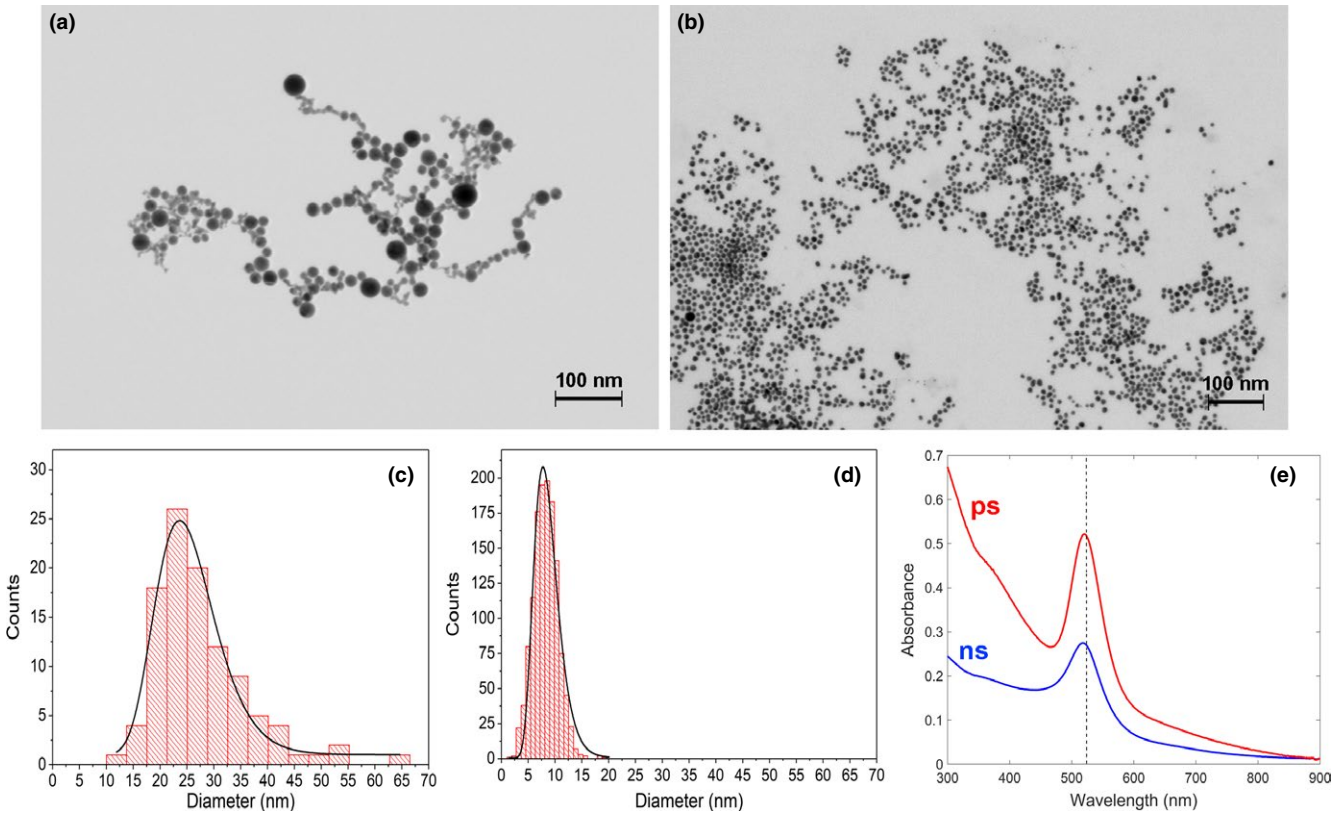

FIGURE 2 STEM image (a) and size distribution (c) of Au NPs prepared at F = 1.5 J/cm^2 for t = 20 minutes (ns irradiations). STEM image (b) and size distribution (d) of Au NPs prepared at F = 1.5 J/cm^2 for t = 5 minutes (ps irradiations). Optical properties of the colloids (e). Au content in colloids prepared by ps-PLAL and ns-PLAL (determined by GF-AAS, see Section), is 312.0 ± 2.5 and 174.5 ± 1.8 μg/ml, respectively

TABLE 1 Histograms fitting results

	Nanosecond	Picosecond
Model	LogNormal	LogNormal
Equation	$y=y_0+\frac{A}{\sqrt{2\pi}wx}e^{-\frac{\left(\ln\left(\frac{x}{x_c}\right)\right)^2}{2w^2}}$	
y_0	1.28 ± 0.76	−2.1 ± 5.4
x_c	24.75 ± 0.42	8.37 ± 0.14
w	0.21 ± 0.02	0.29 ± 0,02
A	313.4 ± 22.0	1077.7 ± 53.2
Reduced chi-square	4.19751	219.16
R^2	0.95387	0.95683

their optical properties were tested by UV–Vis spectroscopy and DLS, and compared to those of freshly prepared colloids. We show in Figure 4 the optical characterization of colloids prepared by ns-PLAL; the results for colloids produced by ps-PLAL are very similar, and are not discussed. After 3 months of storage in dark, at ordinary laboratory conditions, we observed no colour change of the colloids and no evidence of colloid instability. The intensity decrease with time of the SPR (Figure 4a) indicates gravity-induced sedimentation. Accordingly, changes in DLS (Figure 4b) occur at high delay times

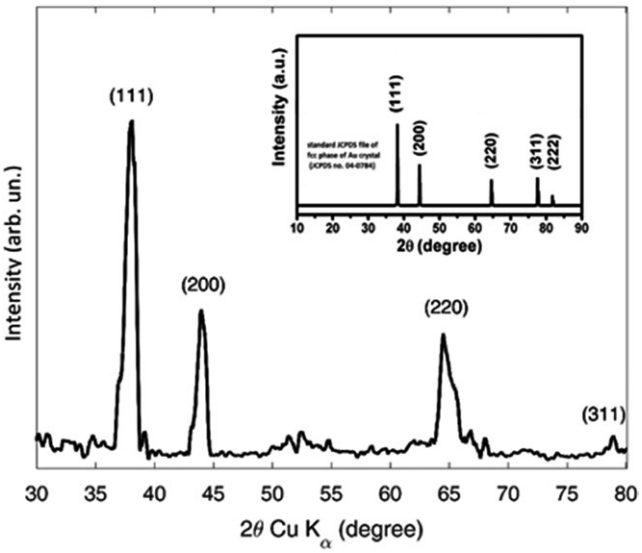

FIGURE 3 XRD pattern of Au NPs prepared by ps-PLAL in demineralized water. A reference XRD from the literature (card JCPDS 04-0784) is shown

that correspond to larger NPs that are more sensitive to gravity. The estimated average size of NPs deduced from DLS reduces from 85 nm (fresh NPs) to about 45 nm (NPs stored for 3 months). Particle

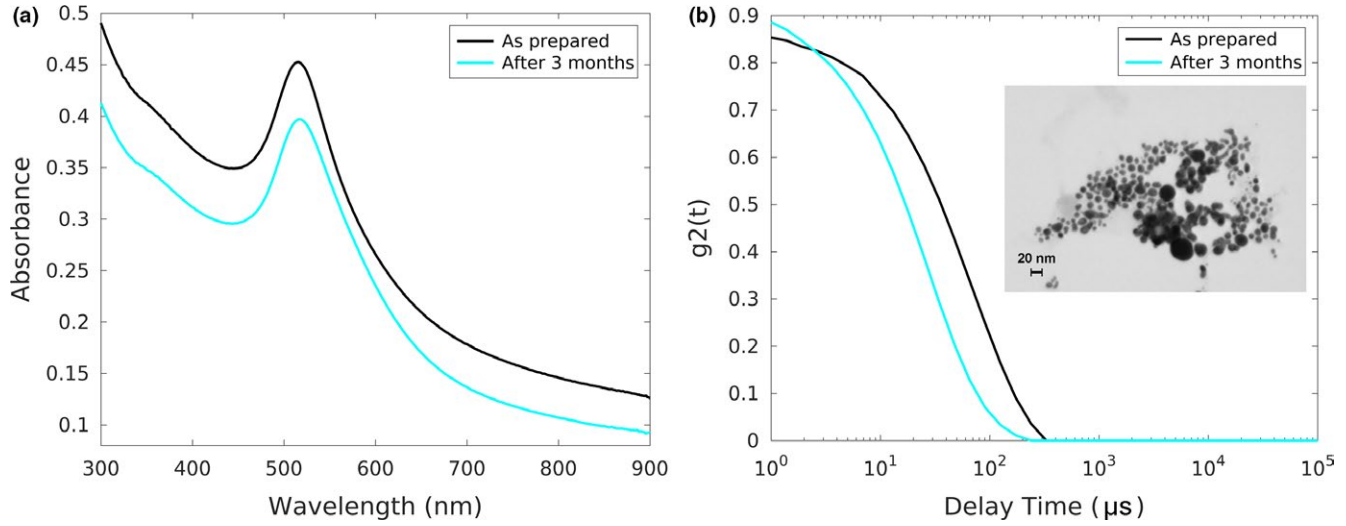

FIGURE 4 (a) UV–Vis optical absorption spectra and (b) DLS correlation curves from Au NPs synthesized by ns-PLAL. Black line: freshly prepared sample; blue line: sample aged 3 months. In the inset, the STEM micrograph of the aged NPs

sedimentation induces a decrease in the optical density of the colloid and a corresponding change in its refractive index. The evident discrepancy between NP size estimated by DLS and STEM data is due to detection limits of DLS in the presence of poly-disperse colloids. Sample polydispersity can affect DLS data because the fraction of non-precipitated large NPs can shield the smaller ones, thus altering the true NP size population (Tomaszewska et al., 2013). Notice that the particle size determined by STEM after three months does not change with respect to the fresh colloids (compare inset of Figure 4b with Figure 2a).

3.3 | SERS substrates made of colloids obtained from ps-PLAL

A fraction of the Au colloids produced by ps-PLAL was ultrasonically sprayed on glass or on (100) Si supports to obtain thin films suitable for SERS measurements. Before performing the SERS tests, we characterized with UV–Vis spectroscopy the films supported on glass, and we examined by SEM the morphologies of the films supported on Si (Figure 5). Comparing the upper absorbance spectrum in Figure 2e (colloids prepared by ps-PLAL) with the homologous spectrum in the inset of Figure 5, we see that the SPR red shifted from 517 nm (Figure 2e) to 522 nm (Figure 5). The FWHM changed from 47 nm (Figure 2e) to 79 nm (Figure 5). Such redshift and broadening of the SPR is ascribed to the clustering of the colloids when they are transferred on the glass support. Indeed, by SEM, we observe surface morphologies on the films sprayed on Si (Figure 5) which differ from the colloid morphologies observed by STEM (Figure 2b): The isolated, small spherical NPs detected by STEM evolve into larger agglomerates consisting of mostly spherical particles observed by SEM (Figure 5). Such an agglomeration process induced by spraying is actually a desirable feature when producing substrates for SERS considering that it fosters the formation of hot-spots (Solis, Taboada, Obelleiro, Liz-Marzán, & García de Abajo, 2017).

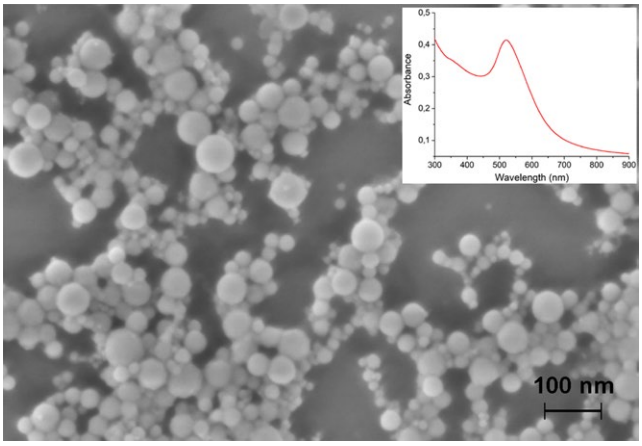

FIGURE 5 SEM image of a representative film obtained ultrasonically spraying on a Si support Au colloids made by ps-PLAL. The associated UV–Vis optical absorbance spectrum is reported in the inset

3.4 | SERS measurements

Before addressing the SERS experiments, we measured as a reference the FT-Raman spectrum of a sample consisting of a 6 mg pharmaceutical tablet of Fycompa, denuded of its protective external coating. In such a sample (namely, the core of the tablet), the API perampanel is mixed with the listed excipients (Figure 6). As shown in Figure 6, among all the declared excipients of Fycompa, the FT-Raman spectrum of lactose monohydrate closely matches the measured spectrum of the sample. The well-resolved Raman features (a–d), which by comparison are not due to lactose monohydrate, are assigned to the API, as the most intense Raman peaks of the other excipients cannot be individually observed and just contribute to the background signal. Thus, based on the qualitative assessment of the FT-Raman data, we conclude that the most abundant excipient in the sample is lactose monohydrate that

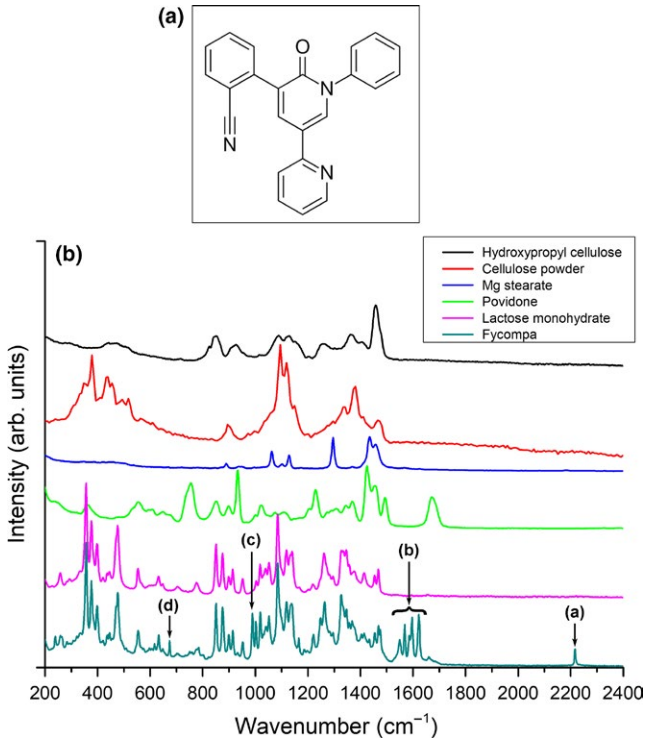

FIGURE 6 (a) Chemical structure of perampanel; (b) FT-Raman spectrum of the core of a Fycompa 6 mg commercial tablet compared with representative FT-Raman spectra of all the excipients declared in the pharmaceutical formulation (http://www.ema.europa.eu/docs/it_IT/document_library/EPAR-_Product_Information/human/002434/WC500130815.pdf). The labels (a–d) mark the Raman features assigned to the active pharmaceutical ingredient, perampanel. See text for details

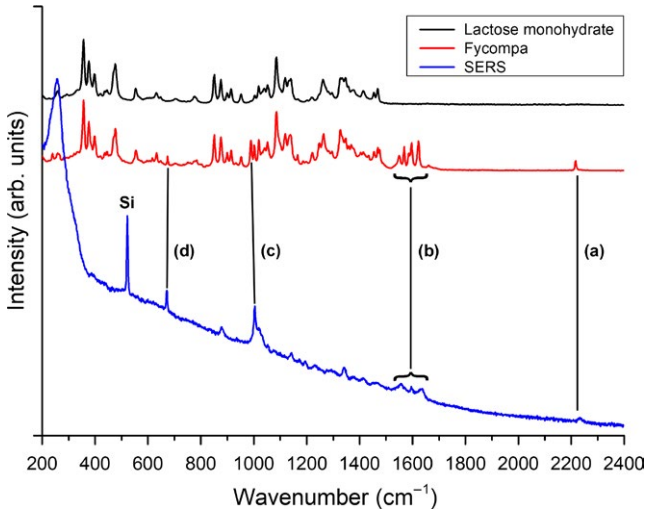

FIGURE 7 SERS spectrum of the methanol extract of perampanel (estimated concentration ≤1.4 × 10^{-3} M; 785 nm excitation wavelength – see Experimental section for details on sample preparation) compared with the FT-Raman spectrum of the Fycompa sample, and with the FT-Raman spectrum of the main excipient (lactose monohydrate). FT-Raman spectra were collected with 1064 nm excitation wavelength

fits the declared composition of the pharmaceutical formulation (http://www.ema.europa.eu/docs/it_IT/document_library/EPAR_Product_Information/human/002434/WC500130815.pdf).

The FT-Raman spectrum of the Fycompa sample shows four distinct features (a–d) that can be attributed with confidence to the API, as they fall in wavenumber ranges where the excipients do not show any strong Raman line. The position of the observed Raman peaks is also consistent with the chemical structure of perampanel (Figure 6a). Line (a) at 2,216 cm^{-1} is assigned to the stretching of the CN bond. The manifold of Raman lines (b) (1,622, 1,597, 1,585, 1,569, 1,550 cm^{-1}) is assigned to aromatic ring stretching modes, and the line (c) at 989 cm^{-1} can be assigned to the breathing of one of the rings of perampanel. Finally, the position of line (d) at 674 cm^{-1} is consistent with an aromatic ring deformation mode. We notice that, to the best of our knowledge, the FT-Raman features of perampanel in Figure 6b are unprecedented.

The SERS spectrum of the methanol extract of the Fycompa sample is shown in Figure 7. Notably, most of the well-defined SERS features observed in Figure 7 can be traced back to the FT-Raman signals of the above-discussed API. We remark that the difference between the position of the CN stretching line (and other API features, as well) in the SERS spectrum, as compared to the FT-Raman, highlights that such signals originate from drug molecules adsorbed on the Au film, that is, not from perampanel recrystallized from the solution. This indicates the successful SERS measurement of perampanel in the solution extracted from the Fycompa sample even in the presence of excipients. This is a promising result in view of clinical applications, where one expects the interference from organic molecules co-extracted with the API from the patient plasma samples.

4 | CONCLUSIONS

In conclusion, by both ns-PLAL and ps-PLAL, it was possible to synthesize Au NPs with no stabilizing agent. The particles have a narrow size distribution and a remarkable long-term stability. Compared to ns-PLAL, ps-PLAL yields smaller NPs in shorter synthesis time, with reduced tendency to agglomerate. Au NPs were tested, allowing to collect the first FT-Raman and SERS spectra of perampanel, an antiepileptic drug of new generation with clinical relevance.

ACKNOWLEDGEMENTS

Funding from Polisocial Award 2013–2014, Project "Controllare l'epilessia nei Paesi in via di sviluppo" is gratefully acknowledged.

REFERENCES

Acacia, N., Barreca, F., Barletta, E., Spadaro, D., Currò, G., & Neri, F. (2010). Laser ablation synthesis of indium oxide nanoparticles

in water. *Applied Surface Science*, *256*, 6918–6922.https://doi.org/10.1016/j.apsusc.2010.05.003

Barcikowski, S., Hahn, A., Kabashin, A. V., & Chichkov, B. N. (2007). Properties of nanoparticles generated during femtosecond laser machining in air and water. *Applied Physics A*, *87*, 47–55.https://doi.org/10.1007/s00339-006-3852-1

Dreaden, E. C., Alkilany, A. M., Huang, X., Murphy, C. J., & El-Sayed, M. A. (2012). The golden age: Gold nanoparticles for biomedicine. *Chemical Society Reviews*, *41*, 2740–2779. https://doi.org/10.1039/C1CS15237H

Fazio, E., & Neri, F. (2013). Nonlinear optical effects from Au nanoparticles prepared by laser plasmas in water. *Applied Surface Science*, *272*, 88–93.https://doi.org/10.1016/j.apsusc.2012.02.147

Fazio, E., Neri, F., Ossi, P. M., Santo, N., & Trusso, S. (2009). Growth process of nanostructured silver films pulsed laser ablated in high-pressure inert gas. *Applied Surface Science*, *255*, 9676.https://doi.org/10.1016/j.apsusc.2009.04.050

Fazio, E., Santoro, M., Lentini, G., Franco, D., Guglielmino, S.P.P., & Neri, F. (2016). Iron oxide nanoparticles prepared by laser ablation: Synthesis, structural properties and antimicrobial activity. *Colloids and Surfaces A: Physicochemical and Engineering Aspects*, *490*, 98–103.https://doi.org/10.1016/j.colsurfa.2015.11.034

Fazio, E., Trusso, S., & Ponterio, R. C. (2013). Surface-enhanced Raman scattering study of organic pigments using silver and gold nanoparticles prepared by pulsed laser ablation. *Applied Surface Science*, *272*, 36–41.https://doi.org/10.1016/j.apsusc.2012.02.070

Hada, H., Yonezawa, Y., Yoshida, A., & Kurakake, A. (1976). Photoreduction of silver ion in aqueous and alcoholic solutions. *Journal of Physical Chemistry*, *80*, 2728–2731.https://doi.org/10.1021/j100566a003

Hamad, A., Li, L., & Liu, Z. (2015). A comparison of the characteristics of nanosecond, picosecond and femtosecond lasers generated Ag, TiO2 and Au nanoparticles in deionised water. *Applied Physics A*, *120*, 1247–1260.https://doi.org/10.1007/s00339-015-9326-6

ICH Harmonised Tripartite Guideline Validation of Analytical Procedures: Text and Methodology Q2(R1) (2005). *International conference of harmonisation of technical requirements for registration of pharmaceuticals for human use*. ICH Official web site, Retrieved from http://www.ich.org/home.html

Indrasekara, A., Paladini, B. J., Naczynski, D. J., Starovoytov, V., Moghe, P. V., & Fabris, L. (2013). Dimeric Gold Nanoparticle Assemblies as Tags for SERS-Based Cancer Detection. *Advanced Healthcare Materials*, *2*, 1370–1376.https://doi.org/10.1002/adhm.201200370

Kelly, R., & Miotello, A. (1996). Comments on explosive mechanisms of laser sputtering. *Applied Surface Science*, *96–98*, 205–215. https://doi.org/10.1016/0169-4332(95)00481-5.

Krauss, G. L., Perucca, E., Ben-Menachem, E., Kwan, P., Shih, J. J., Squillacote, D., … Laurenza, A. (2013). Perampanel, a selective, noncompetitive α-amino-3-hydroxy-5-methyl-4-isoxazolepropionic acid receptor antagonist, as adjunctive therapy for refractory partial-onset seizures: Interim results from phase III, extension study 307. *Epilepsia*, *54*, 126–134. https://doi.org/10.1111/j.1528-1167.2012.03648.x

Kurihara, K., Kizling, J., Stenius, P., & Fendler, J. H. (1983). Laser and pulse radiolytically induced colloidal gold formation in water and in water-in-oil microemulsions. *Journal of the American Chemical Society*, *105*, 25742579.https://doi.org/10.1021/ja00347a011

Mafunè, F., Kohno, J., Takeda, Y., & Kondow, T. (2000). Formation and Size Control of Silver Nanoparticles by Laser Ablation in Aqueous Solution. *The Journal of Physical Chemistry B*, *104*(39), 9111–9117.https://doi.org/10.1021/jp001336y

Momma, C., Chichkov, B. N., Nolte, S., von Alvensleben, F., Tunnermann, A., Welling, H., & Wellegehausen, B. (1996). Short-pulse laser ablation of solid targets. *Optics Communication*, *129*, 134–142.https://doi.org/10.1016/0030-4018(96)00250-7

Ossi, P.M., & Bailini, A. (2008). Cluster growth in an ablation plume propagating through a buffer gas. *Applied Physics A: Materials Science & Processing*, *93*, 645–650.https://doi.org/10.1007/s00339-008-4690-0

Ostendorf, A., Kamlage, G., Klug, U., Korte, F., & Chichkov, B. N. (2005). *Proceedings of SPIE*, *5713*, 1.

Pathak, K., & Povitisky, A. (2008). Plume dynamics and shielding characteristics of nanosecond scale multiple pulse in carbon ablation. *Journal of Applied Physics*, *104*, 113108.https://doi.org/10.1063/1.3032937

Patsalos, P. N. (2015). The clinical pharmacology profile of the new antiepileptic drug perampanel: A novel noncompetitive AMPA receptor antagonist. *Epilepsia*, *56*(1), 12–27.https://doi.org/10.1111/epi.12865

Rogawski, M. A. (2011). Revisiting AMPA receptors as an antiepileptic drug target. *Epilepsy Currents*, *11*, 56–63. https://doi.org/10.5698/1535-7511-11.2.56

Rogawski, M. A., & Hanada, T. (2013). Preclinical pharmacology of perampanel, a selective non-competitive AMPA receptor antagonist. *Acta Neurologica Scandinavica Supplementum*, *197*, 19–24. https://doi.org/10.1111/ane.12100

Sakamoto, M., Fujistuka, M., & Majiam, T. (2009). Light as a construction tool of metal nanoparticles: Synthesis and mechanism. *Journal of Photochemistry and Photobiology C: Photochemistry Reviews*, *10*, 33–56.https://doi.org/10.1016/j.jphotochemrev.2008.11.002

Schwenke, A., Wagener, P., Nolte, S., & Barcikowski, S. (2011). Influence of processing time on nanoparticle generation during picosecond-pulsed fundamental and second harmonic laser ablation of metals in tetrahydrofuran. *Applied Physics A*, *104*, 77–82. https://doi.org/10.1007/s00339-011-6398-9

Sneha, K., Sathishkumar, M., Kim, S., & Yun, Y. S. (2010). Counter ions and temperature incorporated tailoring of biogenic gold nanoparticles. *Process Biochemistry*, *45*, 1450–1458.https://doi.org/10.1016/j.procbio.2010.05.019

Solis, D. M., Taboada, J. M., Obelleiro, F., Liz-Marzán, L. M., & García de Abajo, F. J. (2017). Optimization of nanoparticle-based SERS substrates through large scale realistic simulations. *ACS Photonics*, *4*, 329–337. https://doi.org/10.1021/acsphotonics.6b00786

Tian, L., Fei, M., Tadepalli, S., Morrissey, J. J., Kharasch, E. D., & Singamaneni, S. (2015). Bio-enabled gold superstructures with built-in and accessible electromagnetic hotspots. *Advanced Healthcare Materials*, *4*, 1502–1509. https://doi.org/10.1002/adhm.201500227

Tomaszewska, E., Soliwoda, K., Kadziola, K., Tkacz-Szczesna, B., Celischowsky, G., Cichomski, M., … Grobelny, J. (2013). Detection limits of DLS and UV-Vis spectroscopy in characterization of polydisperse nanoparticles colloids. *Journal of Nanomaterials*, 313081, https://doi.org/10.1155/2013/313081

Zeng, S., Yong, K. T., Roy, I., Dinh, X. Q., Yu, X., & Luan, F. (2011). A review on functionalized gold nanoparticles for biosensing applications. *Plasmonics*, *6*, 491–506.https://doi.org/10.1007/s11468-011-9228-1

How to cite this article: Santoro M, Fazio E, Trusso S, et al. SERS sensing of perampanel with nanostructured arrays of gold particles produced by pulsed laser ablation in water. *Med Devices Sens*. 2018;1:e10003. https://doi.org/10.1002/mds3.10003